C–Cl Bond Activation at Rotated vs Unrotated Dinuclear Site Related to [FeFe]-Hydrogenases

Lucile Chatelain, Federica Arrigoni, Philippe Schollhammer, Giuseppe Zampella

C-Cl bond activation at rotated vs unrotated dinuclear site related to [FeFe]-hydrogenases

Lucile Chatelain,[a] *Federica Arrigoni,*[b] *Philippe Schollhammer,*[a] *and Giuseppe Zampella*[b]

[a] UMR CNRS 6521 Chimie, Electrochimie Moléculaires et Chimie Analytique, Université de Bretagne Occidentale, 6 Avenue Victor le Gorgeu, CS93837, Brest-Cedex 3, 29238, France.

[b] Department of Biotechnology and Bioscience, University of Milano-Bicocca, Piazza della Scienza 2, 20126 Milan, Italy.

ABSTRACT

The novel dinuclear complex related to the [FeFe]-hydrogenases active site, $[Fe_2(\mu\text{-pdt})(\kappa^2\text{-dmpe})_2(CO)_2]$ (**1**), is highly reactive towards chlorinated compounds CH_xCl_{4-x} (x = 1, 2) affording selectively terminal or bridging chloro di-iron isomers through a C-Cl bond activation. DFT calculations suggest a cooperative mechanism involving a formal concerted regioselective chloronium transfer depending on the unrotated or rotated conformation of two isomers of **1**.

The activation of C-Cl bonds by transition metal complexes represents a crucial objective motivated by economic and environmental imperatives, whether for employing chlorocarbons as substrates or facilitating dechlorination processes.[1–10] While numerous mononuclear complexes able to activate small CH_xCl_{4-x} (x = 1, 2) substrates have been reported,[11–15] well-defined polymetallic complexes (generally based on 2nd-3rd row transition metals), which induce

the cleavage of C-Cl bonds of polychlorinated molecules, are more scarce.[16–30] Despite the existence of numerous di-iron complexes inspired by the [FeFe]-hydrogenases metal cofactor, their "promiscuous" activity, i.e., other than that concerning the H^+/H_2 conversion,[31–40] has been little explored.[41–46] The activation of chlorinated organic molecules with such Fe_2 complexes has never been reported. Here we present the reactivity towards polychlorinated molecules of the bis-chelated complex $[Fe_2(\mu\text{-pdt})(\kappa^2\text{-dmpe})_2(CO)_2]$ (**1**) (dmpe: 1,2-bis(dimethylphosphino)ethane; pdt: propanedithiolate), a new example of tetrasubstituted diiron dithiolate complex.[47–55] The cleavage of C-Cl bonds through an unusual cooperative bimetallic mechanism, involving a formal regioselective chloronium transfer, has been investigated by DFT.

1 was prepared as a dark brown powder, in good yields, by UV irradiation (365 nm) of THF or toluene solutions of the hexacarbonyl precursor $[Fe_2(\mu\text{-pdt})(CO)_6]$, in the presence of an excess of dmpe (3-4 equiv.) (Scheme 1).

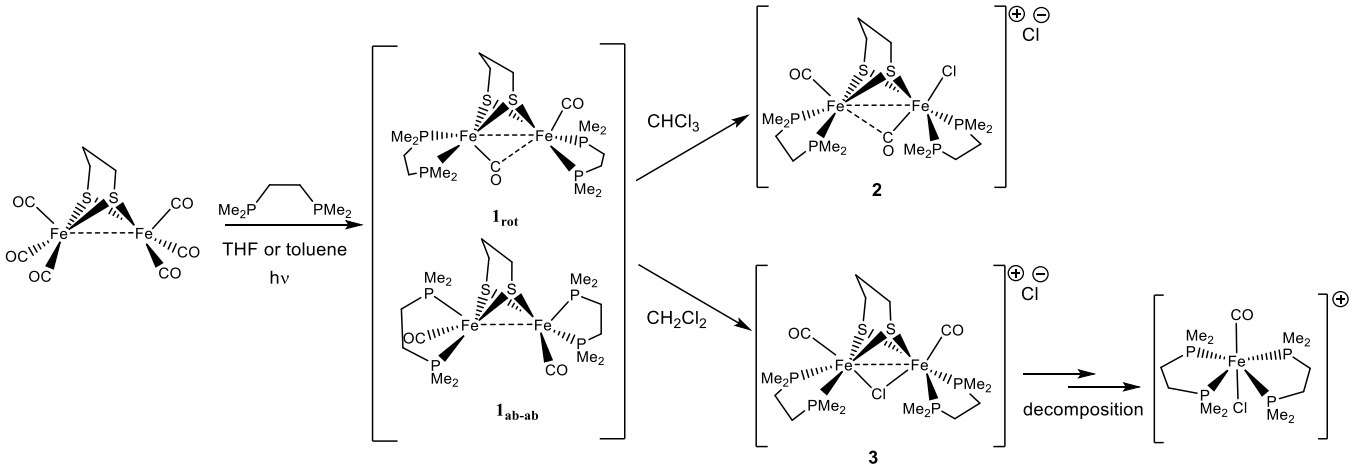

Scheme 1. Syntheses of complexes **1**-**3**

Single crystals of **1**, suitable for an X-ray analysis, grew in saturated hexane solution at room temperature. The solid-state structure revealed that the two dmpe ligands adopt an apical-basal disposition (Fig. 1a). The structure of **1** is typical of $[Fe_2(\mu\text{-SR})_2L_6]$

compounds with a butterfly $\{Fe_2S_2\}$ core.[48,49,51,52,56] The Fe-Fe distance, of 2.5197(6) Å, is shorter than those observed in analogous complexes [2.5678(4)-2.6164(6) Å].[48,49,51,52]

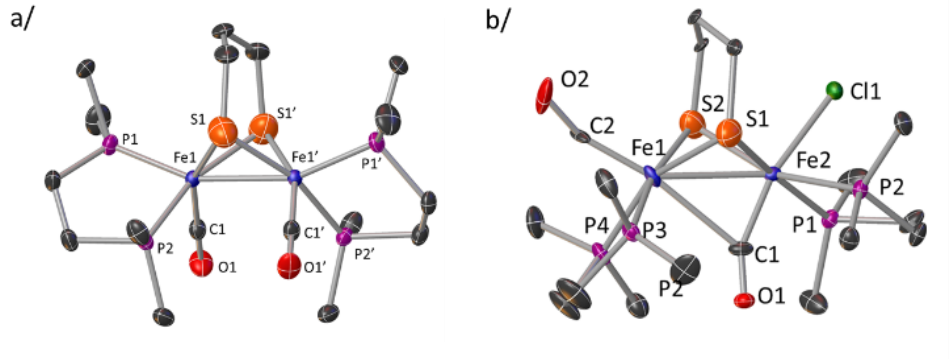

Figure 1 Crystallographic structures of **a/** $[Fe_2(\mu\text{-pdt})(\kappa^2\text{-dmpe})_2(CO)_2]$ (**1**). Atoms labeled with 'are obtained with a 2-fold axis (1-x, +y, ½-z)); **b/** $[Fe_2(\mu\text{-pdt})(\mu\text{-CO})(\kappa^2\text{-dmpe})_2(CO)Cl]Cl.4CHCl_3$ (**2**.$4CHCl_3$). Displacement ellipsoids are drawn at the 40% probability level and disorders, $CHCl_3$ solvent molecules, Cl^- counter ion and hydrogen atoms are omitted for clarity

The ^1H NMR spectrum of a freshly prepared solution of **1** in CD_2Cl_2 showed ill-resolved resonances between 2.27 and 1.42 ppm assigned to the signals of both dmpe and pdt ligands (Fig. S9). The $^{31}P\{^1H\}$ NMR spectrum of **1** in CD_2Cl_2 revealed at room temperature a broad singlet at 60.0 ppm which suggests a fluxional motion of the diphosphine. Upon cooling at 213 K in CD_2Cl_2, this signal splits into two singlets at 69.1 and 52.3 ppm (Fig. S10), which could be attributed to the isomer $\mathbf{1_{ab\text{-}ab}}$ observed in solid state. $^{13}C\{^1H\}$ NMR spectrum at 203K in CD_2Cl_2 (Fig. S12) confirms the symmetry of **1**. It is noteworthy that depending on the solvent, further resonances were detected in the $^{31}P\{^1H\}$ NMR spectrum in addition to the broad signal of **1**, which suggests the presence in solution of an isomer of $\mathbf{1_{ab\text{-}ab}}$. In C_6D_6 and THF-D_8 solution, two additional signals at 78 and 68 ppm were

observed (Fig. S11), which excludes a bis-(dibasal) isomer. Moreover, the IR spectrum of **1** in THF displays two strong ν(CO) bands at 1863 and 1843 cm^{-1} (Fig. S5) which are, as expected, shifted to lower frequencies compared to those of its dppv (cis-1,2-bis(diphenylphosphino)ethylene) analog[51] and very close to that of [Fe_2(μ-pdt)$(PMe_3)_4(CO)_2$].[48] Unlike these latter four-substituted compounds, a third weak band lies at 1799 cm^{-1} in the range of ν(μ-CO) bands.[57–59] To gain further insights into the isomeric stability, a thermodynamic speciation of **1** was carried out by DFT in both CH_2Cl_2 and $CHCl_3$ solvents (Fig. 2 and ESI-section VI).[60–62] Two isoenergetic structures were found as the most stable: a bis-(apical-basal) unrotated isomer $\mathbf{1_{ab\text{-}ab}}$, that resembles the X-ray structure of **1**, and unexpectedly, a bis-(dibasal) rotated form ($\mathbf{1_{rot}}$). The DFT IR νCO)s suggest that the three bands experimentally observed (1795, 1836 and 1856 cm^{-1} in CH_2Cl_2) likely arise from an equilibrium mixture of these two low-energy isomers in solution. Specifically, the band at 1795 cm^{-1} can be assigned to the semi-bridging CO in $\mathbf{1_{rot}}$. No other rotated isomer was found as stable structure. Moreover, calculated ^{31}P NMR chemical shifts of $\mathbf{1_{ab\text{-}ab}}$ and $\mathbf{1_{rot}}$ agree with experimental observations (Fig. S25).

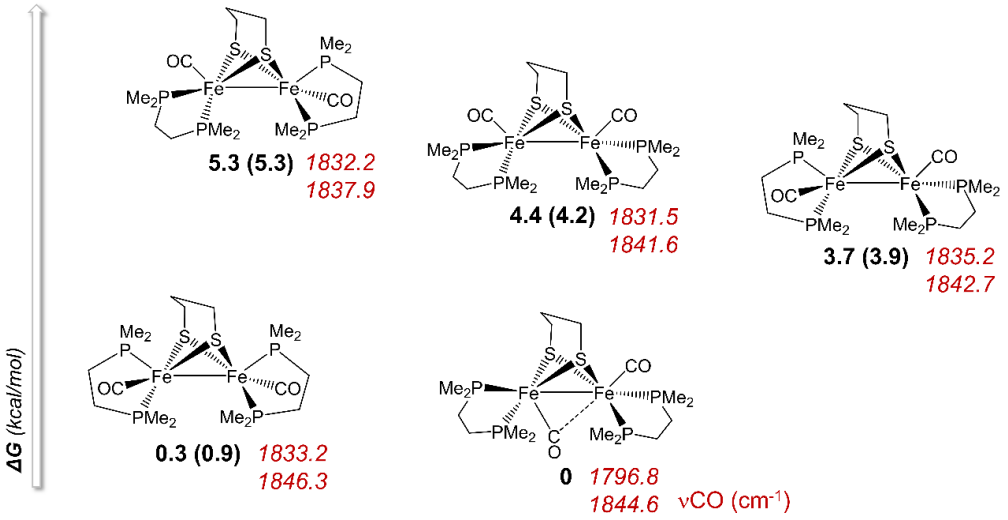

Figure 2. Thermodynamic speciation of **1**. Relative free energies (kcal/mol) in CH_2Cl_2 and $CHCl_3$ (in parenthesis) and ν(CO)s (cm^{-1}, gas phase, red values) are reported.

The dissolution of **1** into $CHCl_3$ (experiments performed both in light and in dark to prevent the formation of halocarbon radicals) afforded serendipitously X-ray quality crystals of $[Fe_2(\mu\text{-pdt})(\mu\text{-CO})(\kappa^2\text{-dmpe})_2(CO)Cl]Cl.4CHCl_3$ **2**.4($CHCl_3$) (Fig. 1b). **2** could be readily and quantitatively prepared, at room temperature, by addition of a drop of $CHCl_3$ to a solution of **1** in hexane, that induced its instant precipitation in excellent yield (96%). Analysis of the volatiles by NMR spectroscopy revealed the presence of a mixture of dechlorinated molecules CH_2Cl_2, $C_2H_2Cl_4$, C_2HCl_3 (ESI-Section VII). The X-ray structure of **2** reveals a cationic $\{Fe_2S_2\}$ core with two dmpe ligands in dibasal position and a bridging CO. A second carbonyl group and a Cl ligand in terminal apical positions complete the Fe coordination sphere. The Fe-Fe distance (2.629(2) Å) is much longer than that of other di-ferrous complexes bearing a bridging CO [2.5135(12)-2.5943(10) Å].[50,55,63,64] The μ-CO ligand adopts a dissymmetrical position (C1-$Fe2_{Cl}$, 1.788(11); C1-$Fe1_{CO}$, 2.430(12) Å) similar to that observed in analogous dissymmetrical compounds.[55,63,64] The presence of a terminal Cl in $[Fe_2(\mu\text{-SR})_2L_6]$ compounds recalls the structure of rare examples of Fe_2 terminal hydride, which are considered as models of a crucial intermediate in the bidirectional H^+/H_2 catalytic conversion induced by the H-cluster.[48,63] The spectroscopic measurements recorded in solution, $^{31}P\{^1H\}$, $^{13}C\{^1H\}$ NMRs and IR (Fig. S3, S16, S17) accord with the X-ray structural determination of **2**.

In CH_2Cl_2, **1** evolves differently than in $CHCl_3$, affording the unstable Cl bridged complex $[Fe_2(\mu\text{-pdt})(\mu\text{-Cl})(\kappa^2\text{-dmpe})_2(CO)_2]Cl$ (**3**), after stirring two days at room temperature, with moderate yields (58%). $^{31}P\{^1H\}$, $^{13}C\{^1H\}$ NMR and IR spectra of **3** suggest a symmetrical bis-

dibasal geometry (Fig. S3, S19, S20), which is similar to those of analogous complexes $[Fe_2(\mu\text{-pdt})(\mu\text{-Cl})(dppR)_2(CO)_2](BF_4)$ (dppR: dppe, dppv), which have been obtained by assembly of two mono-iron precursors.[47] X-ray quality crystals obtained from a solution containing **3** in CH_2Cl_2: THF mixtures allowed to characterize three complexes consisting in $[Fe_2(\mu\text{-pdt})(\mu\text{-Cl})(\kappa^2\text{-dmpe})_2(CO)]^+$ and two mono-iron compounds $[Fe(\kappa^2\text{-dmpe})_2(CO)Cl]^+$ and $[FeCl_4]^{2-}$ arising from the decomposition of **3** in solution. Despite the poor crystallographic data, the connectivity of atoms remains without ambiguity, showing the dinuclear structure $[Fe_2(\mu\text{-pdt})(\mu\text{-Cl})(\kappa^2\text{-dmpe})_2(CO)]^+$ of **3** (Fig. S1).

Furthermore, the absence of interconversion between **2** and **3** over time is puzzling (Fig. S7, S8). To explore the **2** vs **3** stability and understand how the C-Cl bond activation (induced by **1**) leads to different isomers depending on the activated Cl molecule, a thermodynamic speciation of the Cl species and a mechanistic investigation of their formation were performed by DFT. The most stable Cl isomer resulted the Cl-bridging $\mathbf{3_{bb\text{-}bb}}$ (Fig. S26). Other dmpe dispositions are clearly unfavoured. This implies that, starting from $\mathbf{1_{ab\text{-}ab}}$, dmpe ligands must rotate to get $\mathbf{3_{bb\text{-}bb}}$.

Stable isomers of **2** are also favoured with dmpe ligands in dibasal position but the pdt orientation strongly affects the relative energetic stability (from ~8.5 to ~3 kcal/mol). Considering the presence of a chelate at the rotating Fe, a Ray-Dutt twist (pseudo-rhombic -tetragonal- rearrangement of four metal ligands in six-coordinated complexes) as a first step of a hypothetic t-Cl/μ-Cl interconversion is unlikely since it would bring one of the two P atoms (constrained within the chelate structure) at the Fe-Fe region. The μ-Cl/t-Cl interconversion can be conceived as a multi-step mechanism composed by sequential Bailar and Ray-Dutt twists (Fig. S27)[65] that would be thermodynamically feasible ($\Delta G = \pm 3$

kcal/mol), but kinetically impeded (high activation barriers), irrespective of the solvent considered, in agreement with the observation that **2** and **3** do not interconvert (Scheme 1).

DFT clearly suggests that the reaction mechanism is a direct concerted Cl^+ transfer, leading to complexes **2** or **3** and a resulting anion $[RCl_{x-1}]^-$. This would subsequently couple to another solvent molecule with concerted Cl^- release, a process predicted to be thermodynamically facile, considering its strong exergonicity (-60 kcal/mol for CH_2Cl_2 and -48 kcal/mol for $CHCl_3$), as also confirmed by the experimental evidence. Indeed, the products found in the volatiles of the reaction of **1**+$CHCl_3$ confirmed the formation of a $CHCl_2^-$ moiety. A mechanism involving an oxidative addition for the activation of the σ(C-Cl) bond was ruled out due to the high instability of the intermediate species (Fig. S28) and the involvement of a radical Fe(I)(Fe(II) cationic intermediate[66,67] is highly unlikely in reason of the redox behavior of CH_2Cl_2.[68] Sequential (Fig. 3) and concerted (trimolecular) (Fig. S30) mechanisms, involving one or two solvent molecules, respectively, were finally considered. A kinetic preference for the mechanism with a single solvent molecule was evidenced. The energy profiles for the reaction of **1** with CH_2Cl_2 and $CHCl_3$ were determined considering the most stable and isoenergetic $\mathbf{1_{rot}}$ and $\mathbf{1_{ab\text{-}ab}}$. DFT suggests that the Cl-bridged **3** could be formed from $\mathbf{1_{ab\text{-}ab}}$ both in the presence of CH_2Cl_2 or $CHCl_3$ (Fig. 3, left) through a Cl^+ transfer to the Fe-Fe bond only after a preliminary isomerization of $\mathbf{1_{ab\text{-}ab}}$ to $\mathbf{1_{bb\text{-}bb}}$ (TS1 and TS2), while all other alternatives are unfavored (Fig. S29). The formation of $\mathbf{3_{bb\text{-}bb}}$ from $\mathbf{1_{bb\text{-}bb}}$ is exergonic both in CH_2Cl_2 and in $CHCl_3$ with an overall activation barrier of ~14 kcal/mol. μ-Cl formation is more favored in $CHCl_3$ than in CH_2Cl_2 (by ~3 kcal/mol) probably due to the higher stability of the anionic $CHCl_2^-$ vs CH_2Cl^-, formed upon Cl^+ transfer. When considering the rotated isomer $\mathbf{1_{rot}}$, a straight Cl^+ transfer from $CHCl_3$ affords the terminal-Cl complex **2** (Fig. 3, blue

profile) while no Cl^+ transfer in terminal position is observed with CH_2Cl_2 (Fig. 3, orange profile). We ascribe this behavior to the different strength of the C-Cl bond in CH_2Cl_2 (BDE = 79 kcal/mol) vs $CHCl_3$ (BDE =72 kcal/mol).[69] Only two pathways lead to **2** from $\mathbf{1_{rot}}$: the energetically preferred one involves a Cl^+ transfer (TS5) followed by pdt flip (TS6) to form the most stable isomer of **2**. The overall activation barrier for t-Cl formation is 9.7 kcal/mol, compatible with a fast process even under mild temperature conditions and explains the unique formation of **2** in presence of $CHCl_3$.

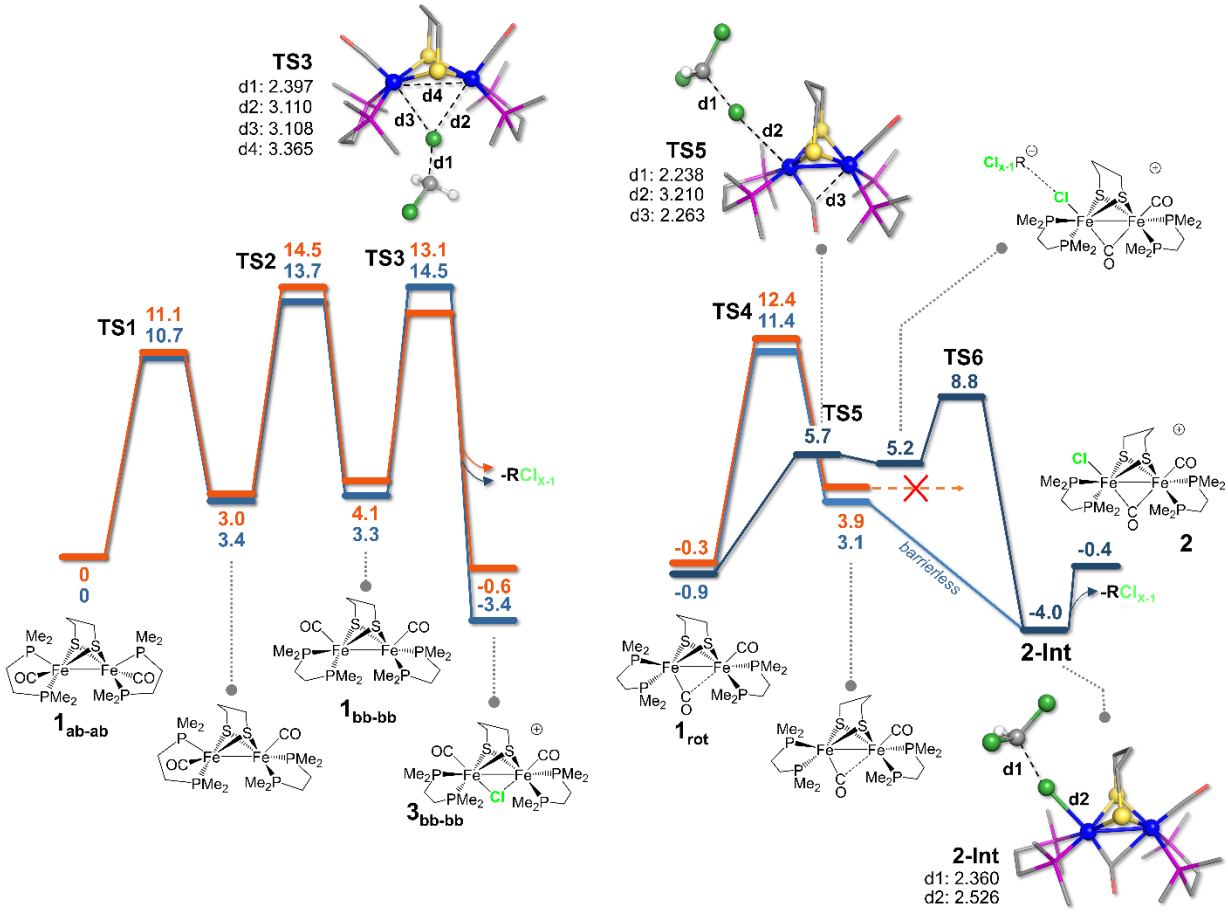

Figure 3. Free energy profiles (in kcal/mol) for the formation of both **3** and **2**, starting from $\mathbf{1_{ab\text{-}ab}}$ (taken as reference) and $\mathbf{1_{rot}}$, respectively. The structures of intermediates and relevant transition states are reported. Orange profiles are calculated in CH_2Cl_2 solvent and in the presence of one explicit CH_2Cl_2 molecule (R = CH_2, X = 2), while blue ones are calculated in $CHCl_3$ with an explicit $CHCl_3$ molecule (R = CH, X = 3). The activation barriers for a-b to b-b isomerization of dmpe are taken from reference[40] and have been recalculated in implicit $CHCl_3$ solvent. Optimized structures of relevant TS's and intermediates are reported: TS3 for CH_2Cl_2, TS5 and 2-Int for $CHCl_3$. Selected

distances in Å. Atoms coloring: C = grey, Fe = blue, P = purple, S = yellow, O = red, Cl = green, H = white. H atoms of the complex have been omitted for clarity. **2** is only formed in $CHCl_3$ and the pathway of its formation goes through the 5.7 TS (not found in the CH_2Cl_2 case). All this implies that $\mathbf{1_{rot}}$ is not a trigger for the stronger C-Cl bond of CH_2Cl_2 (see BDE values provided in the text), but only for the weaker analog bond of $CHCl_3$. On the contrary, in CH_2Cl_2, the right-side pathway indicates that $\mathbf{1_{rot}}$ is not a trigger for the C-Cl bond. This is compatible with the slower formation process of **3**, experimentally observed.

CONCLUSION

In conclusion, the electron-rich **1** is a new example of a 2Fe(I) complex $[Fe_2(\mu\text{-pdt})L_x(CO)_{6-x}]$ for which the coexistence in solution of isoenergetic stereoisomers with unrotated and rotated conformers have been evidenced.[57–59] The control of the unrotated geometry depends on diiron redox state and is still challenging. It remains a crux for having a hydrogenase-like activity.[70,71] Moreover, the reactivity of **1** towards CH_xCl_{4-x} (x = 1, 2) compounds is an original example of bimetallic activation of robust C-Cl bonds at a $\{Fe_2S_2\}$ site that leads to terminal or bridged Cl isomers, which may arise through a concerted regiochemically selective (FeFe site vs Fe apical regions) formal transfer of chloronium. This depends on the unrotated or rotated conformation of **1** and the relative stability of the generated anion $CH_xCl_{3-x}^-$ (x = 1, 2). Finally, these results could be relevant to the treatment and degradation of halogenated organic pollutants. Further investigations on the reactivity of **1** towards other environmentally relevant chlorinated molecules are under way.

ASSOCIATED CONTENT

Supporting Information.

The Supporting Information is available free of charge at https://pubs.acs.org/doi/10.1021/acs.inorgchem.

Protocols for syntheses, NMR, IR, ESI spectra of products, crystallographic and DFT data (DOC)

CCDC 2246265-2246266, 2281641 contain the supplementary crystallographic data for this paper. These data can be obtained free of charge via www.ccdc.cam.ac.uk_request/cif

AUTHOR INFORMATION

Corresponding Authors

Federica Arrigoni – *Department of Biotechnology and Bioscience, University of Milano-Bicocca, Piazza della Scienza 2, 20126 Milan, Italy. @orcid.org / 0000-0003-0691-7517*

E-mail: federica.arrigoni@unimib.it

Lucile Chatelain – *UMR CNRS 6521 Chimie, Electrochimie Moléculaires et Chimie Analytique, Université de Bretagne Occidentale, UFR Sciences et Techniques, 6 Avenue Victor le Gorgeu, CS93837, Brest-Cedex 3, 29238, France. @orcid.org / 0000-0003-4275-6087*

E-mail: lucile.chatelain@univ-brest.fr

Philippe Schollhammer – *UMR CNRS 6521 Chimie, Electrochimie Moléculaires et Chimie Analytique, Université de Bretagne Occidentale, UFR Sciences et Techniques, 6 Avenue Victor le Gorgeu, CS93837, Brest-Cedex 3, 29238, France. @orcid.org / 0000-0001-8161-7878*

E-mail: philippe.schollhammer@univ-brest.fr

Giuseppe Zampella – *Department of Biotechnology and Bioscience, University of Milano-Bicocca, Piazza della Scienza 2, 20126 Milan, Italy. @orcid.org / 0000-0003-0517-6016*

E-mail: giuseppe.zampella@unimib.it

Author Contributions

The manuscript was written through contributions of all authors. All authors have given approval to the final version of the manuscript.

Funding Sources

The research was supported by ANR funding: JCJC OxySplit-H2 (ANR-20-CE07-0027-01).

Notes

ACKNOWLEDGMENT

We are grateful to the 'Service Général des Plateformes, Brest' for NMR experiments and XRD recordings. L. C. is grateful to Dr. J. Pécaut for the help in the crystallographic structure resolution. L.C. thanks the ANR (Agence Nationale de Recherche) for funding the project JCJC OxySplit-H2 (ANR-20-CE07-0027-01).

REFERENCES

§ These values have been calculated using a "simplified" approach according to the equations: $\Delta G = G(C_2H_2Cl_4) + G(Cl^-) - G(CHCl_2^-) - G(CHCl_3)$ and $\Delta G = G(C_2H_4Cl_2) + G(Cl^-) - G(CH_2Cl^-) - G(CH_2Cl_2)$, considering each molecule at infinite distance with respect to the others. Although probably underestimated, these values are compatible with a strongly favored process and with a higher reactivity of CH_2Cl^- vs $CHCl_3^-$.

(1) Jayaraj, R.; Megha, P.; Sreedev, P. Review Article. Organochlorine Pesticides, Their Toxic Effects on Living Organisms and Their Fate in the Environment. *Interdiscipl. Toxicol.* **2017**, *9* (3–4), 90–100. https://doi.org/10.1515/intox-2016-0012.

(2) Volpe, A.; Lopez, A.; Mascolo, G.; Detomaso, A. Chlorinated Herbicide (Triallate) Dehalogenation by Iron Powder. *Chemosphere* **2004**, *57* (7), 579–586. https://doi.org/10.1016/j.chemosphere.2004.06.040.

(3) Singh, S. P.; Bose, P. Reductive Dechlorination of Endosulfan Isomers and Its Metabolites by Zero-Valent Metals: Reaction Mechanism and Degradation Products. *RSC Adv.* **2017**, *7* (44), 27668–27677. https://doi.org/10.1039/C7RA02430D.

(4) He, W. Y.; Fontmorin, J.-M.; Hapiot, P.; Soutrel, I.; Floner, D.; Fourcade, F.; Amrane, A.; Geneste, F. A New Bipyridyl Cobalt Complex for Reductive Dechlorination of Pesticides. *Electrochimica Acta* **2016**, *207*, 313–320. https://doi.org/10.1016/j.electacta.2016.04.170.

(5) Shimakoshi, H.; Hisaeda, Y. A Hybrid Catalyst for Light-Driven Green Molecular Transformations. *ChemPlusChem* **2017**, *82* (1), 18–29. https://doi.org/10.1002/cplu.201600303.

(6) Giedyk, M.; Goliszewska, K.; Gryko, D. Vitamin B12 Catalysed Reactions. *Chem. Soc. Rev.* **2015**, *44* (11), 3391–3404. https://doi.org/10.1039/C5CS00165J.

(7) Tlili, A.; Schranck, J. The Application of Dichloromethane and Chloroform as Reagents in Organic Synthesis. In *Solvents as Reagents in Organic Synthesis: Reactions and Applications*; John Wiley & Sons, Ltd, 2017; pp 125–159. https://doi.org/10.1002/9783527805624.ch4.

(8) Marshall, K. A.; Pottenger, L. H. Chlorocarbons and Chlorohydrocarbons. In *Kirk-Othmer Encyclopedia of Chemical Technology*; John Wiley & Sons, Ltd, 2016; pp 1–29. https://doi.org/10.1002/0471238961.1921182218050504.a01.pub3.

(9) He, C.; Cheng, J.; Zhang, X.; Douthwaite, M.; Pattisson, S.; Hao, Z. Recent Advances in the Catalytic Oxidation of Volatile Organic Compounds: A Review Based on Pollutant Sorts and Sources. *Chem. Rev.* **2019**, *119* (7), 4471–4568. https://doi.org/10.1021/acs.chemrev.8b00408.

(10) Yang, J.; Fan, S.; Li, X.; Tao, Y.; Wang, J.; Chen, G. Highly Efficient Electrocatalysis Dechlorination of Dichloromethane over Single-Atom Cu/Co_3O_4-β Spinel Nanofibers. *Chem. Eng. J.* **2023**, *470*, 144040. https://doi.org/10.1016/j.cej.2023.144040.

(11) Longcake, A.; Lees, M. R.; Senn, M. S.; Chaplin, A. B. Oxidative Addition of C–Cl Bonds to a Rh(PONOP) Pincer Complex. *Organometallics* **2022**, *41* (23), 3557–3567. https://doi.org/10.1021/acs.organomet.2c00400.

(12) de las Heras, L. A.; Esteruelas, M. A.; Oliván, M.; Oñate, E. C–Cl Oxidative Addition and C–C Reductive Elimination Reactions in the Context of the Rhodium-Promoted Direct Arylation. *Organometallics* **2022**, *41* (6), 716–732. https://doi.org/10.1021/acs.organomet.1c00643.

(13) Morrow, T. J.; Gipper, J. R.; Christman, W. E.; Arulsamy, N.; Hulley, E. B. A Terminal Rh Methylidene from Activation of CH_2Cl_2. *Organometallics* **2020**, *39* (13), 2356–2364. https://doi.org/10.1021/acs.organomet.0c00031.

(14) Algarra, A. G.; Galindo, J. C. G.; Puerta, M. C.; Valerga, P.; Jiménez-Tenorio, M. Activation of Dichloromethane by a Bis-NHC Cp*Ru Complex: Formation of a Pentamethyl(Chloromethyl)Cyclopentadiene Ligand. *Organometallics* **2021**, *40* (15), 2405–2408. https://doi.org/10.1021/acs.organomet.1c00340.

(15) Osipova, E. S.; Gulyaeva, E. S.; Kireev, N. V.; Kovalenko, S. A.; Bijani, C.; Canac, Y.; Valyaev, D. A.; Filippov, O. A.; Belkova, N. V.; Shubina, E. S. Fac-to-Mer Isomerization Triggers Hydride Transfer from Mn(I) Complex Fac-[(Dppm)$Mn(CO)_3H$]. *Chem. Commun.* **2022**, *58* (32), 5017–5020. https://doi.org/10.1039/D2CC00999D.

(16) Schollhammer, P.; Pétillon, F. Y.; Talarmin, J.; Muir, K. W.; Fun, H. K.; Chinnakali, K. Halogenation and Alkylation at a $Mo^{III}_2(\mu\text{-}S)$ Site. Crystal Structure of the Metal−Sulfenyl Halide Complex $[Mo_2(\eta^5\text{-}C_5Me_5)_2(\mu\text{-}SMe)_2(\mu\text{-}SI)(CO)_2]I_5$. *Inorg. Chem.* **2000**, *39* (25), 5879–5882. https://doi.org/10.1021/ic000591u.

(17) Ojo, W.-S.; Pétillon, F. Y.; Schollhammer, P.; Talarmin, J. Carbon−Sulfur and Carbon−Halogen Bond Cleavage of Acyclic or Cyclic Thioethers, Thiophenes, and Dihaloalkanes with the Trithiolato-Bridged Cation $[Mo_2Cp_2(\mu\text{-}SMe)_3(MeCN)_2]^+$. *Organometallics* **2010**, *29* (2), 448–462. https://doi.org/10.1021/om900901s.

(18) Platon, M.; Wijaya, N.; Rampazzi, V.; Cui, L.; Rousselin, Y.; Saeys, M.; Hierso, J.-C. Thioetherification of Chloroheteroarenes: A Binuclear Catalyst Promotes Wide Scope and High Functional-Group Tolerance. *Chem. – Eur. J.* **2014**, *20* (39), 12584–12594. https://doi.org/10.1002/chem.201403337.

(19) Murray, H. H.; Porter, L. C.; Fackler, J. P.; Raptis, R. G. Addition of Halogens to $[\{Au(CH_2)_2PPh_2\}_2RX]$ Complexes. The Structures of Cis,Trans-$[\{Au(CH_2)_2PPh_2\}_2(CH_2CF_3)Br_3]$ and Trans,Trans-$[\{Au(CH_2)_2PPh_2\}_2(CHCl_2)Br_2Cl]$. *J. Chem. Soc., Dalton Trans.* **1988**, No. 10, 2669–2674. https://doi.org/10.1039/DT9880002669.

(20) Brunet, J.-J.; Couillens, X.; Daran, J.-C.; Diallo, O.; Lepetit, C.; Neibecker, D. Activation of Dichloromethane by (Phosphane)Orhodium(I) Complexes − X-Ray Structure of $[(PEt_3)_2RhCl_2(\mu\text{-}Cl)_2(\mu\text{-}CH_2)]$. *Eur. J. Inorg. Chem.*

1998, *1998* (3), 349–353. https://doi.org/10.1002/(SICI)1099-0682(199803)1998:3<349::AID-EJIC349>3.0.CO;2-5.

(21) Tejel, C.; Ciriano, M. A.; Oro, L. A.; Tiripicchio, A.; Ugozzoli, F. Bimetallic Reactivity of Dirhodium Compounds Leading to Functionalized Methylene-Bridged Compounds. *Organometallics* **2001**, *20* (8), 1676–1682. https://doi.org/10.1021/om000946h.

(22) Ball, G. E.; Cullen, W. R.; Fryzuk, M. D.; James, B. R.; Rettig, S. J. Oxidative Addition of Dichloromethane to $[(Dppe)Rh]_2(\mu\text{-}Cl)_2$ (Dppe = $Ph_2PCH_2CH_2PPh_2$). X-Ray Structure of $[(Dppe)RhCl]_2(\mu\text{-}Cl)_2(\mu\text{-}CH_2)$. *Organometallics* **1991**, *10* (10), 3767–3769. https://doi.org/10.1021/om00056a058.

(23) Blank, B.; Glatz, G.; Kempe, R. Single and Double C-Cl-Activation of Methylene Chloride by P,N-Ligand Coordinated Rhodium Complexes. *Chem. Asian J.* **2009**, *4* (2), 321–327. https://doi.org/10.1002/asia.200800359.

(24) Ciriano, M. A.; Tena, M. A.; Oro, L. A. Reactions of Chloroform and Gem-Dichlorocarbons with Binuclear Rhodium Complexes Leading to Functionalized Methylene-Bridged Compounds. *J. Chem. Soc., Dalton Trans.* **1992**, No. 13, 2123–2124. https://doi.org/10.1039/DT9920002123.

(25) Tejel, C.; Ciriano, M. A.; López, J. A.; Jiménez, S.; Bordonaba, M.; Oro, L. A. One-Electron versus Two-Electron Mechanisms in the Oxidative Addition Reactions of Chloroalkanes to Amido-Bridged Rhodium Complexes. *Chem. – Eur. J.* **2007**, *13* (7), 2044–2053. https://doi.org/10.1002/chem.200600971.

(26) Mas-Ballesté, R.; Capdevila, M.; Champkin, P. A.; Clegg, W.; Coxall, R. A.; Lledós, A.; Mégret, C.; González-Duarte, P. Diverse Evolution of $[\{Ph_2P(CH_2)nPPh_2\}Pt(\mu\text{-}S)_2Pt\{Ph_2P(CH_2)nPPh_2\}]$ (n = 2, 3) Metalloligands in CH_2Cl_2. *Inorg. Chem.* **2002**, *41* (12), 3218–3229. https://doi.org/10.1021/ic0107173.

(27) Li, Z.; Zheng, W.; Liu, H.; Mok, K. F.; Hor, T. S. A. Interpolymetallic Assembly of d^8–d^{10} Sulfide Aggregates from $[Pt_2(PPh_3)_4(\mu\text{-}S)_2]$ and Group 12 Metals. *Inorg. Chem.* **2003**, *42* (25), 8481–8488. https://doi.org/10.1021/ic034884+.

(28) Yam, V. W.-W.; Yeung, P. K.-Y.; Cheung, K.-K. Unusual Reactivity of a Luminescent Bis-μ-Sulfido Platinum(II) Dimer with Methylene Chloride. X-Ray Structural Characterization of $[Pt_2(\mu\text{-}S)_2(Dppy)_4]$ and $[Pt(Dppy)_2(S_2CH_2)]$(Dppy = 2-Diphenylphosphinopyridine). *J. Chem. Soc., Chem. Commun.* **1995**, No. 2, 267–269. https://doi.org/10.1039/C39950000267.

(29) Gennari, M.; Pécaut, J.; DeBeer, S.; Neese, F.; Collomb, M.-N.; Duboc, C. A Fully Delocalized Mixed-Valence Bis-μ(Thiolato) Dicopper Complex: A Structural and Functional Model of the Biological CuA Center. *Angew. Chem. Int. Ed.* **2011**, *50*, 5662–5666. https://doi.org/10.1002/anie.201100605.

(30) Su, L.; Yang, D.; Zhang, Y.; Wang, B.; Qu, J. Methylene Insertion into an Fe_2S_2 Cluster: Formation of a Thiolate-Bridged Diiron Complex Containing an Fe–CH_2–S Moiety. *Chem. Commun.* **2018**, *54* (93), 13119–13122. https://doi.org/10.1039/C8CC07418F.

(31) Elleouet, C.; Pétillon, F. Y.; Schollhammer, P. Chapter 17 - [FeFe]-Hydrogenases Models. In *Advances in Bioorganometallic Chemistry*; Hirao, T., Moriuchi, T., Eds.; Elsevier, 2019; pp 347–364. https://doi.org/10.1016/B978-0-12-814197-7.00017-0.

(32) Schilter, D.; Camara, J. M.; Huynh, M. T.; Hammes-Schiffer, S.; Rauchfuss, T. B. Hydrogenase Enzymes and Their Synthetic Models: The Role of Metal Hydrides. *Chem. Rev.* **2016**, *116* (15), 8693–8749. https://doi.org/10.1021/acs.chemrev.6b00180.

(33) Kleinhaus, J. T.; Wittkamp, F.; Yadav, S.; Siegmund, D.; Apfel, U.-P. [FeFe]-Hydrogenases: Maturation and Reactivity of Enzymatic Systems and Overview of Biomimetic Models. *Chem. Soc. Rev.* **2021**, *50* (3), 1668–1784. https://doi.org/10.1039/D0CS01089H.

(34) Zhao, X.; Georgakaki, I. P.; Miller, M. L.; Yarbrough, J. C.; Darensbourg, M. Y. H/D Exchange Reactions in Dinuclear Iron Thiolates as Activity Assay Models of Fe−H_2Ase. *J. Am. Chem. Soc.* **2001**, *123* (39), 9710–9711. https://doi.org/10.1021/ja0167046.

(35) Zhao, X.; Chiang, C.-Y.; Miller, M. L.; Rampersad, M. V.; Darensbourg, M. Y. Activation of Alkenes and H_2 by [Fe]-H_2Ase Model Complexes. *J. Am. Chem. Soc.* **2003**, *125* (2), 518–524. https://doi.org/10.1021/ja0280168.

(36) Camara, J. M.; Rauchfuss, T. B. Mild Redox Complementation Enables H_2 Activation by [FeFe]-Hydrogenase Models. *J. Am. Chem. Soc.* **2011**, *133* (21), 8098–8101. https://doi.org/10.1021/ja201731q.

(37) Camara, J. M.; Rauchfuss, T. B. Combining Acid–Base, Redox and Substrate Binding Functionalities to Give a Complete Model for the [FeFe]-Hydrogenase. *Nature Chem* **2012**, *4* (1), 26–30. https://doi.org/10.1038/nchem.1180.

(38) Wang, N.; Wang, M.; Wang, Y.; Zheng, D.; Han, H.; Ahlquist, M. S. G.; Sun, L. Catalytic Activation of H2 under Mild Conditions by an [FeFe]-Hydrogenase Model via an Active μ-Hydride Species. *J. Am. Chem. Soc.* **2013**, *135* (37), 13688–13691. https://doi.org/10.1021/ja408376t.

(39) Ahmed, M. E.; Nayek, A.; Križan, A.; Coutard, N.; Morozan, A.; Ghosh Dey, S.; Lomoth, R.; Hammarström, L.; Artero, V.; Dey, A. A Bidirectional Bioinspired [FeFe]-Hydrogenase Model. *J. Am. Chem. Soc.* **2022**, *144* (8), 3614–3625. https://doi.org/10.1021/jacs.1c12605.

(40) Chatelain, L.; Breton, J.-B.; Arrigoni, F.; Schollhammer, P.; Zampella, G. Geometrical Influence on the Non-Biomimetic Heterolytic Splitting of H_2 by Bio-Inspired [FeFe]-Hydrogenase Complexes: A Rare Example of Inverted Frustrated Lewis Pair Based Reactivity. *Chem. Sci.* **2022**, *13* (17), 4863–4873. https://doi.org/10.1039/D1SC06975F.

(41) Zheng, D.; Wang, N.; Wang, M.; Ding, S.; Ma, C.; Darensbourg, M. Y.; Hall, M. B.; Sun, L. Intramolecular Iron-Mediated C–H Bond Heterolysis with an Assist of Pendant Base in a [FeFe]-Hydrogenase Model. *J. Am. Chem. Soc.* **2014**, *136* (48), 16817–16823. https://doi.org/10.1021/ja5078014.

(42) Zheng, D.; Wang, M.; Wang, N.; Cheng, M.; Sun, L. Effect of Bridgehead Steric Bulk on the Intramolecular C–H Heterolysis of [FeFe]-Hydrogenase Active Site Models Containing a P_2N_2 Pendant Amine Ligand. *Inorg. Chem.* **2016**, *55* (2), 411–418. https://doi.org/10.1021/acs.inorgchem.5b00923.

(43) Cheng, M.; Yu, Y.; Zhou, X.; Luo, Y.; Wang, M. Chemical Versatility of [FeFe]-Hydrogenase Models: Distinctive Activity of $[\mu\text{-}C_6H_4\text{-}1,2\text{-}(\kappa^2\text{-}S)_2][Fe_2(CO)_6]$ for Electrocatalytic CO_2 Reduction. *ACS Catal.* **2019**, *9* (1), 768–774. https://doi.org/10.1021/acscatal.8b03921.

(44) Marx, M.; Mele, A.; Spannenberg, A.; Steinlechner, C.; Junge, H.; Schollhammer, P.; Beller, M. Addressing the Reproducibility of Photocatalytic Carbon Dioxide Reduction. *ChemCatChem* **2020**, *12* (6), 1603–1608. https://doi.org/10.1002/cctc.201901686.

(45) Wang, L.; Fan, F.; Liu, J.; Cheng, M. Homogeneous Electrocatalytic CO_2 Reduction by Hexacarbonyl Diiron Dithiolate Complex Bearing Hydroquinone. *J. Organomet. Chem.* **2021**, *954–955*, 122094. https://doi.org/10.1016/j.jorganchem.2021.122094.

(46) Zhang, F.; Woods, T. J.; Zhu, L.; Rauchfuss, T. B. Inhibition of [FeFe]-Hydrogenase by Formaldehyde: Proposed Mechanism and Reactivity of FeFe Alkyl Complexes. *Chem. Sci.* **2021**, *12* (47), 15673–15681. https://doi.org/10.1039/D1SC05803G.

(47) Song, L.-C.; Hong, D.-J.; Guo, Y.-Q.; Wang, X.-Y. Dinuclear $Fe^{II}Fe^{II}$ Biomimetics for the Oxidized State Active Site of [FeFe]-Hydrogenases: Synthesis, Characterization, and Electrocatalytic H_2 Production. *Organometallics* **2018**, *37* (24), 4744–4752. https://doi.org/10.1021/acs.organomet.8b00750.

(48) Zaffaroni, R.; Rauchfuss, T. B.; Gray, D. L.; De Gioia, L.; Zampella, G. Terminal vs Bridging Hydrides of Diiron Dithiolates: Protonation of Fe_2(Dithiolate)$(CO)_2(PMe_3)_4$. *J. Am. Chem. Soc.* **2012**, *134* (46), 19260–19269. https://doi.org/10.1021/ja3094394.

(49) Realini, F.; Elleouet, C.; Pétillon, F. Y.; Schollhammer, P. Tri- and Tetra-Substituted Derivatives of $[Fe_2(CO)_6$(μ-Dithiolate)] as Novel Dinuclear Platforms Related to the H-Cluster of [FeFe]H_2Ases. *Eur. J. Inorg. Chem.* **2022**, *2022* (19), e202200133. https://doi.org/10.1002/ejic.202200133.

(50) van der Vlugt, J. I.; Rauchfuss, T. B.; Wilson, S. R. Electron-Rich Diferrous–Phosphane–Thiolates Relevant to Fe-Only Hydrogenase: Is Cyanide "Nature's Trimethylphosphane"? *Chem. – Eur. J.* **2006**, *12* (1), 90–98. https://doi.org/10.1002/chem.200500752.

(51) Justice, A. K.; Zampella, G.; Gioia, L. D.; Rauchfuss, T. B. Lewis vs. Brønsted-Basicities of Diiron Dithiolates: Spectroscopic Detection of the "Rotated Structure" and Remarkable Effects of Ethane- vs. Propanedithiolate. *Chem. Commun.* **2007**, No. 20, 2019–2021. https://doi.org/10.1039/B700754J.

(52) Carlson, M. R.; Gray, D. L.; Richers, C. P.; Wang, W.; Zhao, P.-H.; Rauchfuss, T. B.; Pelmenschikov, V.; Pham, C. C.; Gee, L. B.; Wang, H.; Cramer, S. P. Sterically Stabilized Terminal Hydride of a Diiron Dithiolate. *Inorg. Chem.* **2018**, *57* (4), 1988–2001. https://doi.org/10.1021/acs.inorgchem.7b02903.

(53) Carroll, M. E.; Barton, B. E.; Rauchfuss, T. B.; Carroll, P. J. Synthetic Models for the Active Site of the [FeFe]-Hydrogenase: Catalytic Proton Reduction and the Structure of the Doubly Protonated Intermediate. *J. Am. Chem. Soc.* **2012**, *134* (45), 18843–18852. https://doi.org/10.1021/ja309216v.

(54) Li, Q.; Lalaoui, N.; Woods, T. J.; Rauchfuss, T. B.; Arrigoni, F.; Zampella, G. Electron-Rich, Diiron Bis(Monothiolato) Carbonyls: C–S Bond Homolysis in a Mixed Valence Diiron Dithiolate. *Inorg. Chem.* **2018**, *57* (8), 4409–4418. https://doi.org/10.1021/acs.inorgchem.8b00094.

(55) Chouffai, D.; Zampella, G.; Capon, J.-F.; Gioia, L. D.; Goff, A. L.; Pétillon, F. Y.; Schollhammer, P.; Talarmin, J. Electrochemical and Theoretical Studies of the Impact of the Chelating Ligand on the Reactivity of $[Fe_2(CO)_4(\kappa^2$-LL)(μ-Pdt)$]^+$ Complexes with Different Substrates (LL = IMe-CH_2-IMe, Dppe; IMe = 1-Methylimidazol-2-Ylidene). *Organometallics* **2012**, *31* (3), 1082–1091. https://doi.org/10.1021/om201143p.

(56) Li, Y.; Rauchfuss, T. B. Synthesis of Diiron(I) Dithiolato Carbonyl Complexes. *Chem. Rev.* **2016**, *116* (12), 7043–7077. https://doi.org/10.1021/acs.chemrev.5b00669.

(57) Munery, S.; Capon, J.-F.; Gioia, L. D.; Elleouet, C.; Greco, C.; Pétillon, F. Y.; Schollhammer, P.; Talarmin, J.; Zampella, G. New Fe^{I}–Fe^{I} Complex Featuring a Rotated Conformation Related to the [2 Fe]H Subsite of [Fe–Fe] Hydrogenase. *Chem. – Eur. J.* **2013**, *19* (46), 15458–15461. https://doi.org/10.1002/chem.201303316.

(58) Goy, R.; Bertini, L.; Elleouet, C.; Görls, H.; Zampella, G.; Talarmin, J.; De Gioia, L.; Schollhammer, P.; Apfel, U.-P.; Weigand, W. A Sterically Stabilized Fe^{I}–Fe^{I} Semi-Rotated Conformation of [FeFe] Hydrogenase Subsite Model. *Dalton Trans.* **2015**, *44* (4), 1690–1699. https://doi.org/10.1039/C4DT03223C.

(59) Wang, W.; Rauchfuss, T. B.; Moore, C. E.; Rheingold, A. L.; De Gioia, L.; Zampella, G. Crystallographic Characterization of a Fully Rotated, Basic Diiron Dithiolate: Model for the H_{red} State? *Chem. – Eur. J.* **2013**, *19* (46), 15476–15479. https://doi.org/10.1002/chem.201303351.

(60) Arrigoni, F.; Rizza, F.; Bertini, L.; De Gioia, L.; Zampella, G. Toward Diiron Dithiolato Biomimetics with Rotated Conformation of the [FeFe]-Hydrogenase Active Site: A DFT Case Study on Electron-Rich, Isocyanide-Based Scaffolds. *Eur. J. Inorg. Chem.* **2022**, *2022* (17), e202200153. https://doi.org/10.1002/ejic.202200153.

(61) Arrigoni, F.; Bertini, L.; Breglia, R.; Greco, C.; De Gioia, L.; Zampella, G. Catalytic H_2 Evolution/Oxidation in [FeFe]-Hydrogenase Biomimetics: Account from DFT on the Interplay of Related Issues and Proposed Solutions. *New J. Chem.* **2020**, *44* (41), 17596–17615. https://doi.org/10.1039/D0NJ03393F.

(62) Arrigoni, F.; Mohamed Bouh, S.; De Gioia, L.; Elleouet, C.; Pétillon, F. Y.; Schollhammer, P.; Zampella, G. Influence of the Dithiolate Bridge on the Oxidative Processes of Diiron Models Related to the Active Site of [FeFe] Hydrogenases. *Chem. – Eur. J.* **2017**, *23* (18), 4364–4372. https://doi.org/10.1002/chem.201605060.

(63) van der Vlugt, J. I.; Rauchfuss, T. B.; Whaley, C. M.; Wilson, S. R. Characterization of a Diferrous Terminal Hydride Mechanistically Relevant to the Fe-Only Hydrogenases. *J. Am. Chem. Soc.* **2005**, *127* (46), 16012–16013. https://doi.org/10.1021/ja055475a.

(64) Yu, X.; Tung, C.-H.; Wang, W.; Huynh, M. T.; Gray, D. L.; Hammes-Schiffer, S.; Rauchfuss, T. B. Interplay between Terminal and Bridging Diiron Hydrides in Neutral and Oxidized States. *Organometallics* **2017**, *36* (11), 2245–2253. https://doi.org/10.1021/acs.organomet.7b00297.

(65) Zampella, G.; Fantucci, P.; De Gioia, L. DFT Characterization of the Reaction Pathways for Terminal- to μ-Hydride Isomerisation in Synthetic Models of the [FeFe]-Hydrogenase Active Site. *Chem. Commun.* **2010**, *46* (46), 8824. https://doi.org/10.1039/c0cc02821e.

(66) Olsen, M. T.; Rauchfuss, T. B.; Zaffaroni, R. Reaction of Aryl Diazonium Salts and Diiron(I) Dithiolato Carbonyls: Evidence for Radical Intermediates. *Organometallics* **2012**, *31* (8), 3447–3450. https://doi.org/10.1021/om300107s.

(67) Haines, R. J.; Beer, J. A. de; Greatrex, R. Reactions of Metal Carbonyl Derivatives. Part XIX. Halogenation Studies of Di-μ-Alkylthio- and Di-μ-Arylthio-Bis(Tricarbonyliron) and Their Substituted Derivatives. *J. Chem. Soc., Dalton Trans.* **1976**, No. 18, 1749–1757. https://doi.org/10.1039/DT9760001749.

(68) Kotsinaris, A.; Kyriacou, G.; Lambrou, CH. Electrochemical Reduction of Dichloromethane to Higher Hydrocarbons. *J. Appl. Electrochem.* **1998**, *28* (6), 613–616. https://doi.org/10.1023/A:1003202203067.

(69) Senkan, S. M. Combustion of Chlorinated Hydrocarbons. In *Pollutants from Combustion: Formation and Impact on Atmospheric Chemistry*; Vovelle, C., Ed.; NATO Science Series; Springer Netherlands: Dordrecht, 2000; pp 303–338. https://doi.org/10.1007/978-94-011-4249-6_15.

(70) Hsieh, C.-H.; Erdem O.F.; Harman S.D.; Singleton M.L.; Reijerse E.; Lubitz W.; Popescu C.V; Reibenspies J.H.; Scott M. Brothers S.M.; Hall M.B. Darensbourg M.Y., Structural and Spectroscopic Features of Mixed Valent FeIIFeI Complexes and Factors Related to the Rotated Configuration of Diiron Hydrogenase. *J. Am. Chem. Soc.* **2012**, *134*, 13089–13102. https://doi.org/10.1021/ja304866r.

(71) Caroll M.E., Barton B.E., Rauchfuss T.B., Carroll P.J. Synthetic Models for the Active Site of the [FeFe]-Hydrogenase: Catalytic Proton Reduction and the Structure of the Doubly Protonated Intermediate. *J. Am. Chem. Soc.* **2012**, *134*, 18843–18852. https://doi.org/10.1021/ja309216v.

Table of content SYNOPSIS

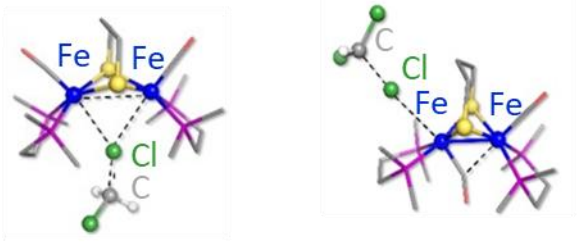

Regioselective chloronium transfer
at rotated or unrotated diiron isomers

An unprecedented bimetallic activation of C-Cl bonds in small chlorinated organic molecules at an electron-rich dithiolate dinuclear site, related to the H-cluster, arises from the cleavage of C-Cl bonds and formal regioselective chloronium transfer.